



MOX-Report No. 55/2016

**Discontinuous Galerkin approximation of flows in
fractured porous media on polytopic grids**

Antonietti, P. F.; Facciola' C.; Russo A.; Verani M.;

MOX, Dipartimento di Matematica
Politecnico di Milano, Via Bonardi 9 - 20133 Milano (Italy)

mox-dmat@polimi.it

<http://mox.polimi.it>

Discontinuous Galerkin approximation of flows in fractured porous media on polytopic grids

Paola F. Antonietti*, Chiara Facciola*, Alessandro Russo# and Marco Verani*

December 15, 2016

* MOX- Laboratory for Modeling and Scientific Computing
Dipartimento di Matematica
Politecnico di Milano
Piazza Leonardo da Vinci 32, 20133 Milano, Italy
`paola.antonietti@polimi.it`, `chiara.facciola@polimi.it`,
`marco.verani@polimi.it`

Dipartimento di Matematica e Applicazioni
Università degli Studi di Milano-Bicocca
Via Cozzi 55, 20125 Milano, Italy
`alessandro.russo@unimib.it`

Abstract

We present a numerical approximation of Darcy's flow through a fractured porous medium which employs discontinuous Galerkin methods on polytopic grids. For simplicity, we analyze the case of a single fracture represented by a $(d - 1)$ -dimensional interface between two d -dimensional subdomains, $d = 2, 3$. We propose a discontinuous Galerkin finite element approximation for the flow in the porous matrix which is coupled with a conforming finite element scheme for the flow in the fracture. Suitable (physically consistent) coupling conditions complete the model. We theoretically analyse the resulting formulation, prove its well-posedness, and derive optimal a priori error estimates in a suitable (mesh-dependent) energy norm. Two-dimensional numerical experiments are reported to assess the theoretical results.

Introduction

Modelling flows in fractured porous media has received increasing attention in the past decades, being fundamental for addressing many

environmental and energy problems, such as water resources management, oil migration tracement, isolation of radioactive waste and ground water contamination, for example. In these applications the flow is strongly influenced by the presence of fractures, which can act as preferential paths (when their permeability is higher than that of the surrounding medium), or as barriers for the flow (when they are filled with low permeable material). A fracture is typically characterized by a small aperture compared to both its length and the size of the domain, and with a different porous structure than the surrounding medium. The task of effectively modelling the interaction between the system of fractures and the porous matrix is particularly challenging. In the following, let us briefly comment on a popular modelling choice to handle such a problem, see, e.g. [35, 27, 5], which consists in treating fractures as $(d - 1)$ -dimensional interfaces between d -dimensional porous matrices, $d = 2, 3$. The development of this kind of reduced models, which can be justified in case of fractures with very small width, has been addressed for single-phase flows in several works, see e.g. [2, 1, 35, 31]. In this paper we adopt the perspective of the single fracture model described in [35], see also [27, 5]. A first version of this model has been introduced in [2] and [1] under the assumption of large permeability in the fracture. In [35] the model has been further generalised to handle also fractures with low permeability. Here, the flow in the porous medium is assumed to be governed by Darcy's law and a suitable reduced version of this law is formulated on the surface modelling the fracture. Physically consistent coupling conditions are added (in strong form) to account for the exchange of fluid between the fracture and the porous medium. The extension of such a coupled model to the case of two-phase flows has been addressed in [32] and [34], while a totally immersed fracture has been considered in [3].

Various numerical methods have been employed in the literature for the approximation of the resulting coupled bulk-fracture model. In this respect, one of the main issues is the construction of the computational grid. Roughly speaking, numerical methods can be classified depending on the interaction between the bulk and the fracture meshes: the computational grid can be either conforming (i.e. matching/aligned) or non-conforming (i.e. non-matching/non-aligned) with the fracture network. In more traditional approaches the bulk meshes are usually chosen to be aligned with the fractures and to be made of simplicial elements. Some examples can be found in [2, 31, 35], where mixed finite element schemes have been employed for the discretization. However, in realistic cases, the geometrical conformity of the bulk mesh to the fracture can either lead to low-quality elements or to very

fine grids, and the process of grid generation might become unaffordable from the computational view point, especially in three-dimensions. Indeed, porous media are often characterised by complicated geometries, i.e. large networks of fractures, which may also intersect with small angles or be nearly coincident. An alternative strategy consists in the use of non-conforming discretizations, where the fractures are allowed to arbitrarily cut the bulk grid. This allows for the choice of a fairly regular mesh in the bulk. We mention in particular [27, 32], where an approximation employing eXtended Finite Element Method (XFEM) has been proposed.

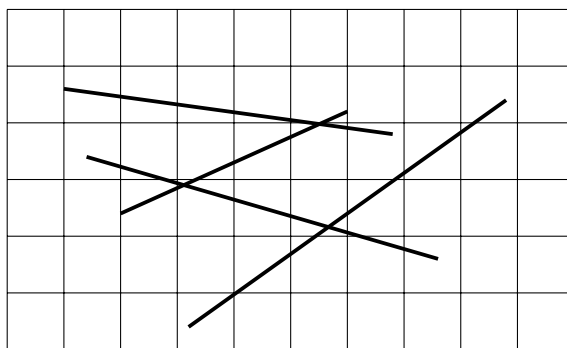


Figure 1: A two-dimensional example of fracture network cutting a Cartesian grid

A good compromise with respect to the above issues is represented by methods based on computational meshes consisting of general polytopic elements (polygons in two dimensions and polyhedra in three dimensions). First a (possibly structured) bulk grid is generated independently of the fracture networks, secondly the elements are cut according to the fracture geometry, see Figure 1 for a representative example. The above approach leads to a grid that

- (i) is aligned with the fracture network;
- (ii) contains possibly arbitrarily shaped elements in the surrounding of fractures;
- (iii) is regular far from fractures.

Beyond the simplicity of generating the computational grid based on employing the previously described approach, one of the main advantages of polytopal decompositions over standard simplicial grids is that, even on relatively simple geometries, the average number of elements needed to discretize complicated domains is lower [6, 7]. This advantage becomes even

more evident whenever the domain presents complex geometrical features (large number of fractures, fractures intersecting with small angles, etc.) and the bulk grid is chosen to be matching with the interfaces. Recently, a mixed approximation based on the use of conforming polygonal meshes and Mimetic Finite Differences (MFD) has been explored in [5]. We also mention a promising framework to treat flows in systems of fracture networks introduced in [17, 18, 16, 19, 15, 30].

The aim of this paper is to employ Discontinuous Galerkin (DG) finite elements on polytopic grids to discretize the coupled bulk-fracture problem stemming from the modelling of flows in fractured porous media. The inherited flexibility of DG methods in handling arbitrarily shaped, non-necessarily matching, grids and elementwise variable polynomial orders represents, in fact, the ideal setting to handle such kind of problems that typically feature a high-level of geometrical complexity. Discontinuous Galerkin methods were first introduced in the early 1970s (see for example [36, 29, 12, 42, 9]) as a technique to numerically solve partial differential equations. They have been successfully developed and applied to hyperbolic, elliptic and parabolic problems arising from a wide range of applications: various examples can be found, for example, in [13, 25, 26, 20, 33, 37, 28]. We refer in particular to [10] for a unified presentation and analysis of classical DG methods for elliptic problems.

More specifically, the choice of DG methods for addressing the problem of the flow in a fractured porous medium arises quite spontaneously in view of the discontinuous nature of the solution at the matrix-fracture interface. However, this is not the only motivation to employ DG methods in this specific context. Indeed, our differential model is based on the primal form of the Darcy's equations for both the bulk and fracture flows, which are coupled with suitable conditions at the interface. These coupling conditions can be naturally formulated using jump and average operators, so that DG methods turn out to be a very natural and powerful tool for efficiently handling the coupling of the two problems, which is indeed naturally embedded in the variational formulation. In this paper we propose a discretization which combines a DG approximation for the problem in the bulk with a conforming finite element approximation in the fracture. The use of conforming finite elements to discretize the equations in the fracture is made just for the sake of simplicity, other discretization techniques can be employed and our approach is general enough to take into account straightforwardly also such cases. For the DG approximation of the problem

in the bulk we will refer in particular to [24, 23, 4] and [21], where an *hp*-version interior penalty Discontinuous Galerkin method is presented for the numerical solution of second-order elliptic partial differential equations on polytopic grids, see also [22] for a review. This method is characterized by a specific choice of the interior penalty parameter, which allows for the use of polytopic meshes made of elements with edges/faces that may be in arbitrary number (potentially unlimited) and whose measure may be arbitrarily small [21]. Clearly, this is naturally well suited to handle complicated networks of fractures. We analyse the resulting method and prove optimal a priori error estimates, which we numerically test in a two-dimensional setting.

The paper is structured as follows. In Section 1 we introduce the governing equations for the coupled problem. The problem is then written in a weak form in Section 2, where we also prove its well-posedness. In Section 3 we introduce the DG discretization on polytopic grids of the coupled problem and state some technical results (in particular inverse estimates which are sharp with respect to element facet degeneration) in order to prove its well-posedness. In Section 4 we derive a priori error estimates in a suitable (mesh-dependent) norm, starting from approximation results valid for general polytopic elements. Finally, in Section 5 we present two-dimensional numerical experiments assessing the validity of the theoretical error estimates.

1 Model problem

Throughout the paper we will employ the following notation. For an open, bounded domain $D \subset \mathbb{R}^d$, $d = 2, 3$, we denote by $H^s(D)$ the standard Sobolev space of order s , for a real number $s \geq 0$. For $s = 0$, we write $L^2(D)$ in place of $H^0(D)$. The usual norm on $H^s(D)$ is denoted by $\|\cdot\|_{H^s(D)}$ and the usual seminorm by $|\cdot|_{H^s(D)}$. Furthermore, we will denote by $\mathbb{P}_k(D)$ the space of polynomials of *total* degree less than or equal to $k \geq 1$ on D . The symbol \lesssim (and \gtrsim) will signify that the inequalities hold up to multiplicative constants which are independent of the discretization parameters, but might depend on the physical parameters.

In the following we present the governing equations for our model, which is a variant of the model derived in [35], where the coupling conditions are imposed in a weak sense. The flow of an incompressible fluid through a fractured d -dimensional porous medium, $d = 2, 3$, can be described by the

following three ingredients:

1. the governing equations for the flow in the porous medium;
2. the governing equations for the flow in the fractures;
3. a set of physically consistent conditions which couple the problems in the bulk and fractures along their interfaces.

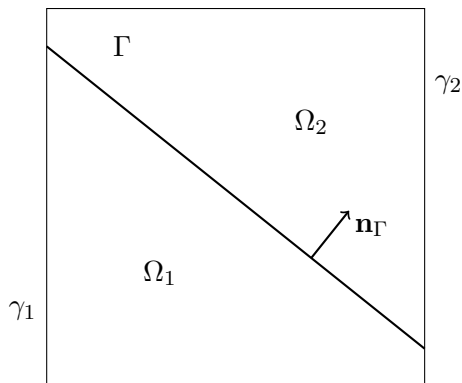


Figure 2: The subdomains Ω_1 and Ω_2 separated by the fracture Γ considered as an interface.

For simplicity, we will assume that there is only one fracture in the porous medium and that the fracture cuts the domain exactly into two disjoint connected subregions (see Figure 2 for a two-dimensional example), following the approach of [27] and [5]. The extension to a network of fractures can be treated analogously, while the case of an immersed fracture is more complex to be analysed [3] and will be the subject of future research. Let $\Omega \subset \mathbb{R}^d$, $d = 2, 3$, be an open, bounded, convex polygonal/polyhedral domain representing the porous matrix. We suppose that the fracture is a $(d - 1)$ -dimensional C^∞ manifold $\Gamma \subset \mathbb{R}^{d-1}$, $d = 2, 3$, whose measure satisfies $|\Gamma| = \mathcal{O}(1)$, and assume that Γ separates Ω into two connected subdomains, which are disjoint, i.e., $\Omega \setminus \Gamma = \Omega_1 \cup \Omega_2$ with $\Omega_1 \cap \Omega_2 = \emptyset$. For $i = 1, 2$, we denote by γ_i the part of boundary of Ω_i shared with the boundary of Ω , i.e., $\gamma_i = \partial\Omega_i \cap \partial\Omega$. We denote by \mathbf{n}_i , $i = 1, 2$ the unit normal vector to Γ pointing outwards from Ω_i and, for a (regular enough) scalar-valued function v and a (regular enough) vector-valued function $\boldsymbol{\tau}$, we define the standard

jump and *average* operators across Γ as

$$\begin{aligned} \{v\} &= \frac{1}{2}(v_1 + v_2) & \llbracket v \rrbracket &= v_1 \mathbf{n}_1 + v_2 \mathbf{n}_2, \\ \{\boldsymbol{\tau}\} &= \frac{1}{2}(\boldsymbol{\tau}_1 + \boldsymbol{\tau}_2) & \llbracket \boldsymbol{\tau} \rrbracket &= \boldsymbol{\tau}_1 \cdot \mathbf{n}_1 + \boldsymbol{\tau}_2 \cdot \mathbf{n}_2, \end{aligned} \quad (1)$$

where the subscript $i = 1, 2$ denotes the restriction to the subdomain Ω_i . Moreover we denote by \mathbf{n}_Γ the normal unit vector on Γ with a fixed orientation from Ω_1 to Ω_2 , so that we have $\mathbf{n}_\Gamma = \mathbf{n}_1 = -\mathbf{n}_2$.

1.1 Governing equations

According to the above discussion, we suppose that the flow in the bulk is governed by Darcy's law. Let $\boldsymbol{\nu} = \boldsymbol{\nu}(x) \in \mathbb{R}^{d \times d}$ be the bulk permeability tensor, which satisfies the following regularity assumptions:

- (i) $\boldsymbol{\nu}$ is a symmetric, positive definite tensor whose entries are bounded, piecewise continuous real-valued functions;
- (ii) $\boldsymbol{\nu}$ is uniformly bounded from below and above, i.e.,

$$\mathbf{x}^T \mathbf{x} \lesssim \mathbf{x}^T \boldsymbol{\nu} \mathbf{x} \lesssim \mathbf{x}^T \mathbf{x} \quad \forall \mathbf{x} \in \mathbb{R}^d. \quad (2)$$

Given a function $f \in L^2(\Omega)$ representing a source term and $g \in H^{1/2}(\partial\Omega)$, the motion of an incompressible fluid in each domain Ω_i , $i = 1, 2$, with pressure p_i is described by:

$$-\nabla \cdot (\boldsymbol{\nu}_i \nabla p_i) = f_i \quad \text{in } \Omega_i, \quad i = 1, 2, \quad (3a)$$

$$p_i = g_i \quad \text{on } \gamma_i, \quad i = 1, 2. \quad (3b)$$

Here we have denoted by $\boldsymbol{\nu}_i$ and f_i , the restrictions of $\boldsymbol{\nu}$ and f to Ω_i , $i = 1, 2$, respectively, and by g_i the restriction of g to γ_i , $i = 1, 2$ (for simplicity, we have imposed Dirichlet boundary conditions on both γ_1 and γ_2).

The second ingredient for the model is represented by the governing equations for the fracture flow. In our model the fracture is treated as a $(d - 1)$ -dimensional manifold immersed in a d -dimensional object. If we assume that the fractures are filled by a porous medium with different porosity and permeability than the surroundings, Darcy's law can be used also for modelling the flow along the fractures [14]. The reduced model is then obtained through a process of averaging across the fracture: in

the beginning the fracture is treated as a d -dimensional subdomain of Ω , that separates it into two disjoint subdomains. Then Darcy's equations are written on the fracture in the normal and tangential components and the tangential component is integrated along the thickness $\ell_\Gamma > 0$ of the fracture domain, which is typically some orders of magnitude smaller than the size of the domain. We refer to [35] for a rigorous derivation of the reduced mathematical model. Note that in [35] this averaging process is carried out for the flow equations written in mixed form. Here, we consider the corresponding model in primal form.

The fracture flow is then characterized by the fracture permeability tensor $\boldsymbol{\nu}_\Gamma$, which is assumed to satisfy the same regularity assumptions as those satisfied by the bulk permeability $\boldsymbol{\nu}$ and to have a block-diagonal structure of the form

$$\boldsymbol{\nu}_\Gamma = \begin{bmatrix} \boldsymbol{\nu}_\Gamma^n & 0 \\ 0 & \boldsymbol{\nu}_\Gamma^\tau \end{bmatrix}, \quad (4)$$

when written in its normal and tangential components. Here, $\boldsymbol{\nu}_\Gamma^\tau \in \mathbb{R}^{(d-1) \times (d-1)}$ is a positive definite, uniformly bounded tensor (it reduces to a positive number for $d = 2$) representing the tangential component of the permeability of the fracture.

Setting $\partial\Gamma = \Gamma \cap \partial\Omega$, and denoting by p_Γ the fracture pressure, the governing equations for the fracture flow read

$$-\nabla_\tau \cdot (\boldsymbol{\nu}_\Gamma^\tau \ell_\Gamma \nabla_\tau p_\Gamma) = f_\Gamma + \llbracket -\boldsymbol{\nu} \nabla p \rrbracket \quad \text{in } \Gamma, \quad (5a)$$

$$p_\Gamma = g_\Gamma \quad \text{on } \partial\Gamma, \quad (5b)$$

where $f_\Gamma \in L^2(\Gamma)$, $g_\Gamma \in H^{1/2}(\partial\Gamma)$ and ∇_τ and $\nabla_\tau \cdot$ denote the tangential gradient and divergence operators, respectively. Equation (5a) represents Darcy's law in the direction tangential to the fracture, where a source term $\llbracket -\boldsymbol{\nu} \nabla p \rrbracket$ is introduced to take into account the contribution of the subdomain flows to the fracture flow [35]. For the sake of simplicity, we impose Dirichlet boundary conditions at the boundary $\partial\Gamma$ of the fracture Γ .

Finally, following [35], we provide the interface conditions to couple problems (3a)-(3b) and (5a)-(5b). Let ξ be a positive real number, $\xi \neq \frac{1}{2}$, that will be chosen later on. The coupling conditions are given by

$$-2\{\boldsymbol{\nu} \nabla p\} \cdot \mathbf{n}_\Gamma = \beta_\Gamma (p_1 - p_2) \quad \text{on } \Gamma, \quad (6a)$$

$$-\llbracket \boldsymbol{\nu} \nabla p \rrbracket = \alpha_\Gamma (\{p\} - p_\Gamma) \quad \text{on } \Gamma, \quad (6b)$$

where

$$\beta_\Gamma = \frac{1}{2\eta_\Gamma}, \quad \alpha_\Gamma = \frac{2}{\eta_\Gamma(2\xi - 1)}, \quad (7)$$

and $\eta_\Gamma = \frac{\ell_\Gamma}{\nu_\Gamma^n}$, ν_Γ^n being the normal component of the fracture permeability tensor, see (4). Note that the coupling conditions are formulated employing jump and average operators. This turns out to be convenient for employing DG methods in the discretization.

In conclusion, the coupled model problem reads:

$$\begin{aligned} -\nabla \cdot (\nu_i \nabla p_i) &= f_i && \text{in } \Omega_i, \quad i = 1, 2, \\ p_i &= g_i && \text{on } \gamma_i, \quad i = 1, 2, \\ -\nabla_\tau \cdot (\nu_\Gamma^\tau \ell_\Gamma \nabla_\tau p_\Gamma) &= f_\Gamma + \llbracket -\nu \nabla p \rrbracket && \text{in } \Gamma, \\ p_\Gamma &= g_\Gamma && \text{on } \partial\Gamma, \\ -2\{\nu \nabla p\} \cdot \mathbf{n}_\Gamma &= \beta_\Gamma(p_1 - p_2) && \text{on } \Gamma, \\ -\llbracket \nu \nabla p \rrbracket &= \alpha_\Gamma(\{p\} - p_\Gamma) && \text{on } \Gamma. \end{aligned} \quad (8)$$

Note that the introduction of the parameter ξ yields a family of models, see [35] for more details.

2 Weak formulation and its well-posedness

In this section we present a weak formulation of our model problem (8) where the coupling conditions (6a)-(6b) are imposed in a weak sense, and prove its well-posedness. For the sake of simplicity we will assume that *homogeneous* Dirichlet boundary conditions are imposed for both the bulk and fracture problems, i.e., $g_i = 0$, $i = 1, 2$, and $g_\Gamma = 0$. The extension to the general non-homogeneous case is straightforward. We introduce the following spaces

$$V^b = \{p = (p_1, p_2) \in V_1^b \times V_2^b\}, \quad V^\Gamma = H_0^1(\Gamma) \cap H^s(\Gamma),$$

where we define, for $i = 1, 2$ and $s \geq 1$, $V_i^b = H^s(\Omega_i) \cap H_{0,\gamma_i}^1(\Omega_i)$, with $H_{0,\gamma_i}^1(\Omega_i) = \{q \in H^1(\Omega_i) \text{ s.t. } q|_{\gamma_i} = 0\}$.

Next we introduce the bilinear forms $\mathcal{A}_b : V^b \times V^b \rightarrow \mathbb{R}$,

$\mathcal{A}_\Gamma : V^\Gamma \times V^\Gamma \rightarrow \mathbb{R}$ and $\mathcal{I} : (V^b \times V^\Gamma) \times (V^b \times V^\Gamma) \rightarrow \mathbb{R}$ defined as

$$\begin{aligned} \mathcal{A}_b(p, q) &= \sum_{i=1}^2 \int_{\Omega_i} \boldsymbol{\nu} \nabla p_i \cdot \nabla q_i, & \mathcal{A}_\Gamma(p_\Gamma, q_\Gamma) &= \int_\Gamma \boldsymbol{\nu}_\Gamma^\tau \ell_\Gamma \nabla p_\Gamma \cdot \nabla q_\Gamma, \\ \mathcal{I}((p, p_\Gamma), (q, q_\Gamma)) &= \int_\Gamma \beta_\Gamma \llbracket p \rrbracket \cdot \llbracket q \rrbracket + \int_\Gamma \alpha_\Gamma (\{p\} - p_\Gamma) (\{q\} - q_\Gamma), \end{aligned}$$

where α_Γ and β_Γ are defined as in (7). Clearly, the bilinear forms $\mathcal{A}_b(\cdot, \cdot)$ and $\mathcal{A}_\Gamma(\cdot, \cdot)$ take into account the problems in the bulk and in the fracture, respectively, while $\mathcal{I}(\cdot, \cdot)$ takes into account the interface conditions (6). We also introduce the linear functional $\mathcal{L}_b : V^b \rightarrow \mathbb{R}$ defined as $\mathcal{L}_b(q) = \sum_{i=1}^2 \int_{\Omega_i} f q_i$, and the linear functional $\mathcal{L}_\Gamma : V^\Gamma \rightarrow \mathbb{R}$ defined as $\mathcal{L}_\Gamma(q_\Gamma) = \int_\Gamma f_\Gamma q_\Gamma$, that represent the source terms in the bulk and fracture, respectively.

With the above notation, the weak formulation of our model problem reads as follows: Find $(p, p_\Gamma) \in V^b \times V^\Gamma$ such that, for all $(q, q_\Gamma) \in V^b \times V^\Gamma$

$$\mathcal{A}((p, p_\Gamma), (q, q_\Gamma)) = \mathcal{L}(q, q_\Gamma), \quad (9)$$

where $\mathcal{A} : (V^b \times V^\Gamma) \times (V^b \times V^\Gamma) \rightarrow \mathbb{R}$ is defined as the sum of the bilinear forms just introduced:

$$\mathcal{A}((p, p_\Gamma), (q, q_\Gamma)) = \mathcal{A}_b(p, q) + \mathcal{A}_\Gamma(p_\Gamma, q_\Gamma) + \mathcal{I}((p, p_\Gamma), (q, q_\Gamma)),$$

and the linear operator $\mathcal{L} : V^b \times V^\Gamma \rightarrow \mathbb{R}$ is defined as

$$\mathcal{L}(q, q_\Gamma) = \mathcal{L}_b(q) + \mathcal{L}_\Gamma(q_\Gamma).$$

Next, we show that formulation (9) is well-posed. To this aim we introduce the following norm on $V^b \times V^\Gamma$:

$$\begin{aligned} \|(q, q_\Gamma)\|_{\mathcal{E}}^2 &= \sum_{i=1}^2 \|\boldsymbol{\nu}_i^{1/2} \nabla q_i\|_{L^2(\Omega_i)}^2 + \|(\boldsymbol{\nu}_\Gamma^\tau \ell_\Gamma)^{1/2} \nabla q_\Gamma\|_{L^2(\Gamma)}^2 \\ &\quad + \|\beta_\Gamma^{1/2} \llbracket q \rrbracket\|_{L^2(\Gamma)}^2 + \|\alpha_\Gamma^{1/2} (\{q\} - q_\Gamma)\|_{L^2(\Gamma)}^2. \end{aligned} \quad (10)$$

This is clearly a norm if $\alpha_\Gamma \geq 0$. Since $\alpha_\Gamma = \frac{2}{\eta_\Gamma(2\xi-1)}$, see (7), from now on, we will assume that $\xi > 1/2$. We remark that the same condition on the parameter ξ has been found also in [35] and [5].

Theorem 2.1. *Let $\xi > 1/2$. Then, problem (9) is well-posed.*

Proof. We show that $\mathcal{A}(\cdot, \cdot)$ is continuous and coercive on $V^b \times V^\Gamma$ equipped with the norm (10), as well as $\mathcal{L}(\cdot)$ is continuous on $V^b \times V^\Gamma$ with respect to the same norm. Then, existence and uniqueness of the solution, as well as linear dependence on the data, follow directly from Lax-Milgram's lemma. Coercivity is straightforward, as we clearly have that $\mathcal{A}((q, q_\Gamma), (q, q_\Gamma)) = \|(q, q_\Gamma)\|_{\mathcal{E}}^2$ for any $(q, q_\Gamma) \in V^b \times V^\Gamma$. On the other hand, continuity is a direct consequence of Cauchy-Schwarz inequality, while continuity of $\mathcal{L}(\cdot)$ on $V^b \times V^\Gamma$ is guaranteed by the regularity of the forcing term f . \square

3 Numerical discretization

In this section we present a numerical discretization of our problem which combines a Discontinuous Galerkin approximation on general polytopic elements for the problem in the bulk, with a conforming finite element approximation in the fracture (see Remark 2 below). DG methods result to be very convenient for handling the discontinuity of the bulk pressure across the fracture, as well as the coupling of the bulk-fracture problems, which has been formulated using jump and average operators. As a result, we can employ the tools offered by DG methods to prove the well-posedness of our discrete method (see Proposition 3.6, below). In particular, we will adopt the techniques developed in [24, 23, 4, 21], where an hp -version interior penalty discontinuous Galerkin method for the numerical solution of elliptic problems on polytopic meshes has been proposed and analysed. This method is characterised by a specific choice of the interior penalty parameter, which allows for face-degeneration. In [24, 23, 4] it is assumed that the number of edges/faces of each mesh element is uniformly bounded. In [21, 8] this assumption is no longer required (i.e., elements with an arbitrary number of possibly degenerating faces/edges are admitted).

We start with the introduction of some useful notation. We consider a family of meshes \mathcal{T}_h made of disjoint open *polygonal/polyhedral* elements which are aligned with the fracture Γ , so that any element $E \in \mathcal{T}_h$ cannot be cut by Γ . Note that, since Ω_1 and Ω_2 are disjoint, each element E belongs exactly to one of the two subdomains. In order to admit hanging nodes, following [24, 23, 4], we introduce the concept of mesh *interfaces*, which are defined to be the intersection of the $(d-1)$ -dimensional facets of neighbouring elements. In the case when $d = 2$, the interfaces of an element $E \in \mathcal{T}_h$ simply consists of line segments. For $d = 3$, we assume that it is possible to subdivide each interface into a set of co-planar triangles. We then use the terminology “face” (or edge) to refer to a $(d-1)$ - dimensional simplex (line segment for $d = 2$ or triangle

for $d = 3$), which forms part of the interface of an element. Note that for $d = 2$ face and interface of an element $E \in \mathcal{T}_h$ coincide. Following [24, 23, 4], for $d = 3$ we assume that, for each mesh interface, a sub-triangulation into faces is provided. Notice that no limitation is imposed on either the number of faces of each polygon $E \in \mathcal{T}_h$ or the relative size of element faces compared to its diameter.

Clearly each mesh \mathcal{T}_h induces a subdivision of the fracture Γ into faces, that we will denote by Γ_h . Moreover, we denote by \mathcal{F}_h the set of all open interfaces of the decomposition \mathcal{T}_h if $d = 2$, and the union of all open triangles belonging to the sub-triangulation of all mesh interfaces if $d = 3$ (so that \mathcal{F}_h is always defined as a set of $(d - 1)$ -dimensional simplices). Moreover, we write

$$\mathcal{F}_h = \mathcal{F}_h^I \cup \mathcal{F}_h^B \cup \Gamma_h,$$

where \mathcal{F}_h^B is the set of boundary faces and \mathcal{F}_h^I is the set of interior faces not belonging to the fracture. For each element $E \in \mathcal{T}_h$, we denote by $|E|$ its measure and by h_E its diameter and we set $h = \max_{E \in \mathcal{T}_h} h_E$. Finally, given an element $E \in \mathcal{T}_h$, for any face/edge $F \subset \partial E$ we define \mathbf{n}_F as the unit normal vector on F that points outside E . We can then define the standard jump and average operators across an edge $F \in \mathcal{F}_h$ for (regular enough) scalar and vector-valued functions similarly to (1).

Given a partition \mathcal{T}_h of the domain, we denote by $H^s(\mathcal{T}_h)$, $s \geq 1$, the standard broken Sobolev space.

With the aim of building a DG-conforming finite element approximation, we choose to set the discrete problem in the finite-dimensional spaces

$$\begin{aligned} V_h^b &= \{q_h \in L^2(\Omega) : q_h|_E \in \mathbb{P}_{k_E}(E) \forall E \in \mathcal{T}_h\}, & k_E &\geq 1, \forall E \in \mathcal{T}_h \\ V_h^\Gamma &= \{q_h^\Gamma \in C^0(\Gamma) : q_h^\Gamma|_F \in \mathbb{P}_k(F) \forall F \in \Gamma_h\} & k &\geq 1. \end{aligned}$$

Note that to each element $E \in \mathcal{T}_h$ is associated the polynomial degree k_E . We also remark that the polynomial degrees in the bulk and fracture discrete spaces just defined are chosen independently.

Next, we introduce the bilinear forms $\mathcal{A}_b^{DG} : V_h^b \times V_h^b \rightarrow \mathbb{R}$ and

$\mathcal{I}^{DG} : (V_h^b \times V_h^\Gamma) \times (V_h^b \times V_h^\Gamma) \rightarrow \mathbb{R}$, defined as follows

$$\begin{aligned} \mathcal{A}_b^{DG}(p_h, q_h) &= \sum_{E \in \mathcal{T}_h} \int_E \boldsymbol{\nu} \nabla p_h \cdot \nabla q_h - \sum_{F \in \mathcal{F}_h \setminus \Gamma_h} \int_F \{\boldsymbol{\nu} \nabla p_h\} \cdot \llbracket q_h \rrbracket \\ &\quad - \sum_{F \in \mathcal{F}_h \setminus \Gamma_h} \int_F \{\boldsymbol{\nu} \nabla q_h\} \cdot \llbracket p_h \rrbracket + \sum_{F \in \mathcal{F}_h \setminus \Gamma_h} \int_F \sigma_F \llbracket p_h \rrbracket \cdot \llbracket q_h \rrbracket, \\ \mathcal{I}^{DG}((p_h, p_h^\Gamma), (q_h, q_h^\Gamma)) &= \sum_{F \in \Gamma_h} \int_F \beta_\Gamma \llbracket p_h \rrbracket \cdot \llbracket q_h \rrbracket + \sum_{F \in \Gamma_h} \int_F \alpha_\Gamma (\{p_h\} - p_h^\Gamma) (\{q_h\} - q_h^\Gamma). \end{aligned}$$

The non-negative function $\sigma \in L^\infty(\mathcal{F}_h \setminus \Gamma_h)$ is the *discontinuity penalization parameter* ($\sigma_F = \sigma|_F$, for $F \in \mathcal{F}_h \setminus \Gamma_h$). The precise definition of σ will be presented in Lemma 3.4 below. Finally we define the linear functional $\mathcal{L}_b^{DG} : V_h^b \rightarrow \mathbb{R}$ as

$$\mathcal{L}_b^{DG}(q_h) = \sum_{E \in \mathcal{T}_h} \int_E f q_h.$$

Remark 1. Since we are imposing homogeneous boundary conditions, \mathcal{L}_b^{DG} has the same structure of the linear functional \mathcal{L}_b previously defined. In general, for $g \neq 0$, \mathcal{L}_b^{DG} contains some additional terms:

$$\mathcal{L}_b^{DG}(q_h) = \sum_{E \in \mathcal{T}_h} \int_E f q_h + \sum_{F \in \mathcal{F}_h^B} \int_F (-\boldsymbol{\nu} \nabla q_h \cdot \mathbf{n}_F + \sigma_F q_h) g.$$

The DG discretization of problem (9) reads as follows: Find $(p_h, p_h^\Gamma) \in V_h^b \times V_h^\Gamma$ such that

$$\mathcal{A}_h((p_h, p_h^\Gamma), (q_h, q_h^\Gamma)) = \mathcal{L}_h(q_h, q_h^\Gamma) \quad \forall (q_h, q_h^\Gamma) \in V_h^b \times V_h^\Gamma, \quad (11)$$

where $\mathcal{A}_h : (V_h^b \times V_h^\Gamma) \times (V_h^b \times V_h^\Gamma) \rightarrow \mathbb{R}$ is defined as

$$\mathcal{A}_h((p_h, p_h^\Gamma), (q_h, q_h^\Gamma)) = \mathcal{A}_b^{DG}(p_h, q_h) + \mathcal{A}_\Gamma(p_h^\Gamma, q_h^\Gamma) + \mathcal{I}^{DG}((p_h, p_h^\Gamma), (q_h, q_h^\Gamma)),$$

and $\mathcal{L}_h : V_h^b \times V_h^\Gamma \rightarrow \mathbb{R}$ is defined as

$$\mathcal{L}_h(q_h, q_h^\Gamma) = \mathcal{L}_b^{DG}(q_h) + \mathcal{L}_\Gamma(q_h^\Gamma).$$

Note that the discrete bilinear form \mathcal{A}_h has the same structure as the bilinear form \mathcal{A} previously defined, being the sum of three different components, each representing a specific part of the problem.

We now want to consider the stability and the error analysis of formulation (11). Since the formulation employs general polytopes, we will first introduce some technical results to treat such kind of discretizations, cf. [24, 23, 4, 21, 8].

3.1 Trace inverse estimates and approximation results

Trace inverse estimates bound the the norm of a polynomial on an element's face/edge by the norm on the element itself. They are at the base of the stability and error analysis of DG methods. The use of grids made of general polytopic elements presents challenges on a number of points. Indeed, in contrast to the case when standard-shaped elements are employed, shape-regular polytopes may admit an arbitrary number of faces/edges and the measure of the faces/edges may potentially be much smaller than the measure of the element itself. In order to obtain an inverse estimate valid on polygons/polyhedra which is sharp with respect to facet degeneration and holds true even when the number of faces/edges is unbounded, taking as a reference [21], we make the following assumption on the mesh:

Assumption 3.1. [21] *For any $E \in \mathcal{T}_h$, there exists a set of non-overlapping (not necessarily shape-regular) d -dimensional simplices $\{S_E^i\}_{i=1}^{n_E}$ contained in E , such that $\bar{F} = \partial\bar{E} \cap \bar{S}_E^i$, for any face $F \subseteq \partial E$, and*

$$h_E \lesssim \frac{d|S_E^i|}{|F|}, \quad i = 1, \dots, n_E. \quad (12)$$

Here, the hidden constant is independent of the discretization parameters, the number of faces of the element n_E , and the face measure.

Note that this assumption does not give any restriction on the number of faces per element nor on the measure of the faces. This is a generalization of the setting presented in [24, 23, 4], where a uniform bound on the number of the element faces was assumed. We also underline that the union of simplices S_E^i does *not* have to cover, in general, the whole element E , that is

$$\cup_{i=1}^{n_E} \bar{S}_E^i \subseteq \bar{E}.$$

In the following, for simplicity and clarity we shall write S_E^F instead of S_E^i .

First, we recall a classical hp -version inverse estimate valid for generic simplices [41].

Lemma 3.2. *Let $S \subset \mathbb{R}^d$ be a simplex, and let $v \in \mathbb{P}_k(S)$. Then, for each $F \subset \partial S$ we have*

$$\|v\|_{L^2(F)}^2 \leq \frac{(k+1)(k+d)}{d} \frac{|F|}{|S|} \|v\|_{L^2(S)}^2.$$

The inverse estimate for polytopic elements is then obtained using Assumption 3.1 as in [21], Lemma 4.1, and [8, 22]. The proof is reported here for completeness.

Lemma 3.3. *Let E be a polygon/polyhedron satisfying Assumption 3.1 and let $v \in \mathbb{P}_{k_E}(E)$. Then, we have*

$$\|v\|_{L^2(\partial E)}^2 \lesssim \frac{k_E^2}{h_E} \|v\|_{L^2(E)}^2, \quad (13)$$

where the hidden constant depends on the dimension d , but it is independent of the discretization parameters and of the number of faces of the element.

Proof. The proof follows immediately if we apply Lemma 3.2 to each simplex $S_E^F \subset E$ from Assumption 3.1, together with (12). More in detail, we have

$$\begin{aligned} \|v\|_{L^2(\partial E)}^2 &= \sum_{F \subset \partial E} \|v\|_{L^2(F)}^2 \lesssim k_E^2 \sum_{F \subset \partial E} \frac{|F|}{|S_E^F|} \|v\|_{L^2(F)}^2 \lesssim \frac{k_E^2}{h_E} \|v\|_{L^2(\cup_{F \subset \partial E} S_E^F)}^2 \\ &\leq \frac{k_E^2}{h_E} \|v\|_{L^2(E)}^2. \end{aligned}$$

□

Note that the estimate bounds the L^2 -norm of the polynomial on the whole boundary of E , not just on one of its edges/faces. This will be of fundamental importance in the analysis.

3.2 Well-posedness of the discrete formulation

We can now proceed with the stability analysis of our method. For simplicity, we suppose that the permeability tensors $\boldsymbol{\nu}$ and $\boldsymbol{\nu}_\Gamma$ are piecewise constant on mesh elements, i.e., $\boldsymbol{\nu}|_E \in [\mathbb{P}_0(E)]^{d \times d}$ for all $E \in \mathcal{T}_h$, and $\boldsymbol{\nu}_\Gamma|_F \in [\mathbb{P}^0(F)]^{(d-1) \times (d-1)}$ for all $F \in \Gamma_h$. In the following, we will employ the notation $\bar{\boldsymbol{\nu}}_E = |\sqrt{\boldsymbol{\nu}|_E}|_2^2$, where $|\cdot|_2$ denotes the l_2 -norm.

Following [24, 23, 4, 21], we base our analysis on the introduction of an appropriate *inconsistent* formulation for the problem in the bulk. To this

end we introduce the following extension of the forms \mathcal{A}_b^{DG} and \mathcal{L}_b^{DG} :

$$\begin{aligned}\tilde{\mathcal{A}}_b^{DG}(p, q) &= \sum_{E \in \mathcal{T}_h} \int_E \nu \nabla p \cdot \nabla q - \sum_{F \in \mathcal{F}_h \setminus \Gamma_h} \int_F \{\nu \Pi_2(\nabla p)\} \cdot \llbracket q \rrbracket \\ &\quad - \sum_{F \in \mathcal{F}_h \setminus \Gamma_h} \int_F \{\nu \Pi_2(\nabla q)\} \cdot \llbracket p \rrbracket + \sum_{F \in \mathcal{F}_h \setminus \Gamma_h} \sigma_F \int_F \llbracket p \rrbracket \cdot \llbracket q \rrbracket, \\ \tilde{\mathcal{L}}_b^{DG}(q) &= \sum_{E \in \mathcal{T}_h} \int_E f q + \left[\sum_{F \in \mathcal{F}_h^B} \int_F (-\nu \Pi_2(\nabla q) \cdot \mathbf{n}_F + \sigma_F q) g \right],\end{aligned}$$

where the integral between square brackets vanishes if we consider homogeneous boundary conditions. Here $\Pi_2 : [L^2(\Omega)]^d \rightarrow [V_h^b]^d$ denotes the orthogonal L^2 -projection onto the bulk finite element space $[V_h^b]^d$. It follows that these forms are well defined on the space $V^b(h) = V_h^b + V^b$, since the terms $\{\nu \Pi_2(\nabla q)\}$ and $\{\nu \Pi_2(\nabla p)\}$ are traces of elementwise polynomial functions. Moreover, it is clear that

$$\tilde{\mathcal{A}}_b^{DG}(p_h, q_h) = \mathcal{A}_b^{DG}(p_h, q_h) \quad \text{for all } q_h, p_h \in V_h^b$$

and

$$\tilde{\mathcal{L}}_b^{DG}(q_h) = \mathcal{L}_b^{DG}(q_h) \quad \text{for all } q_h \in V_h^b.$$

Thereby, $\tilde{\mathcal{A}}_b^{DG}(\cdot, \cdot)$ and $\tilde{\mathcal{L}}_b^{DG}(\cdot)$ are extensions of $\mathcal{A}_b^{DG}(\cdot, \cdot)$ and $\mathcal{L}_b^{DG}(\cdot)$ to $V^b(h) \times V^b(h)$ and $V^b(h)$, respectively. Hence, we may rewrite our discrete problem (11) in the following *equivalent* form:

Find $(p_h, p_h^\Gamma) \in V_h^b \times V_h^\Gamma$ such that

$$\tilde{\mathcal{A}}_h((p_h, p_h^\Gamma), (q_h, q_h^\Gamma)) = \tilde{\mathcal{L}}_h(q_h, q_h^\Gamma) \quad \forall (q_h, q_h^\Gamma) \in V_h^b \times V_h^\Gamma, \quad (14)$$

where $\tilde{\mathcal{A}}_h$ is obtained from \mathcal{A}_h by replacing the bilinear form $\mathcal{A}_b^{DG}(\cdot, \cdot)$ with its inconsistent version $\tilde{\mathcal{A}}_b^{DG}(\cdot, \cdot)$, and $\tilde{\mathcal{L}}_h$ is obtained by replacing the linear operator $\mathcal{L}_b^{DG}(\cdot)$ with $\tilde{\mathcal{L}}_b^{DG}(\cdot)$. We remark that formulation (14) is no longer consistent due to the discrete nature of the L^2 -projection operator Π_2 .

Before proving that formulation (14) is well-posed, we state (and prove) some auxiliary results, see Lemma 3.4 and 3.5 below. We primarily introduce the following norm on $V^b(h) \times V_h^\Gamma$

$$\|(q, q_h^\Gamma)\|_{\tilde{\mathcal{E}}_h}^2 = \|q\|_{DG}^2 + \|q_h^\Gamma\|_\Gamma^2 + \|(q, q_h^\Gamma)\|_{\mathcal{I}}^2, \quad (15)$$

where

$$\begin{aligned} \|q\|_{DG}^2 &= \|\boldsymbol{\nu}^{1/2} \nabla_h q\|_{L^2(\Omega)}^2 + \sum_{F \in \mathcal{F}_h \setminus \Gamma_h} \|\sigma_F^{1/2} \llbracket q \rrbracket\|_{L^2(F)}^2, \\ \|q_h^\Gamma\|_\Gamma^2 &= \|(\boldsymbol{\nu}_\Gamma^\tau \ell_\Gamma)^{1/2} \nabla_h q_h^\Gamma\|_{L^2(\Gamma)}^2, \\ \|(q, q_h^\Gamma)\|_{\mathcal{I}}^2 &= \sum_{F \in \Gamma_h} \|\beta_\Gamma^{1/2} \llbracket q \rrbracket\|_{L^2(F)}^2 + \sum_{F \in \Gamma_h} \|\alpha_\Gamma^{1/2} (\{q\} - q_h^\Gamma)\|_{L^2(F)}^2. \end{aligned}$$

It is easy to show that $\|\cdot\|_{DG}$ is a norm if $\sigma_F > 0$ for all $F \in \mathcal{F}_h \setminus \Gamma_h$ and that $\|\cdot\|_{\mathcal{I}}$ is a norm if $\alpha_\Gamma \geq 0$ (that is $\xi > 1/2$).

In order to obtain coercivity and continuity for the bilinear form $\tilde{\mathcal{A}}_b^{DG}(\cdot, \cdot)$ we need to appropriately choose the discontinuity-penalization parameter. Taking as a reference [24, 23, 4, 21], we state and prove the following result. Note that, for the proof, Assumption 3.1 will play a fundamental role.

Lemma 3.4. *Let $\sigma : \mathcal{F}_h \setminus \Gamma_h \rightarrow \mathbb{R}^+$ be defined facewise by*

$$\sigma(\mathbf{x}) = \sigma_0 \begin{cases} \max_{E \in \{E^+, E^-\}} \frac{\bar{\nu}_E(k_E+1)(k_E+d)}{h_E}, & \text{if } \mathbf{x} \in F \in \mathcal{F}_h^I, \bar{F} = \partial \bar{E}^+ \cap \partial \bar{E}^- \\ \frac{\bar{\nu}_E(k_E+1)(k_E+d)}{h_E}, & \text{if } \mathbf{x} \in F \in \mathcal{F}_h^B, \bar{F} = \partial \bar{E} \cap \partial \bar{\Omega}, \end{cases} \quad (16)$$

with $\sigma_0 > 0$ independent of k_E , $|E|$ and $|F|$. Then, if Assumption 3.1 holds, the bilinear form $\tilde{\mathcal{A}}_b^{DG}(\cdot, \cdot)$ is continuous on $V^b(h) \times V^b(h)$ and, provided that σ_0 is sufficiently large, it is also coercive on $V^b(h) \times V^b(h)$, i.e.,

$$\tilde{\mathcal{A}}_b^{DG}(p, q) \lesssim \|q\|_{DG} \|p\|_{DG}, \quad \tilde{\mathcal{A}}_b^{DG}(q, q) \gtrsim \|q\|_{DG}^2,$$

for any $q, p \in V^b(h)$.

Proof. For the proof we follow [24] and [21]. We start with coercivity. For any $q \in V^b(h)$,

$$\begin{aligned} \tilde{\mathcal{A}}_b^{DG}(q, q) &= \|q\|_{DG}^2 - 2 \sum_{F \in \mathcal{F}_h \setminus \Gamma_h} \int_F \{\boldsymbol{\nu} \Pi_2(\nabla q)\} \cdot \llbracket q \rrbracket \\ &= I + II. \end{aligned}$$

In order to bound term II, we employ Cauchy-Schwarz's, triangular and Young's inequalities to obtain

$$\begin{aligned}
\sum_{F \in \mathcal{F}_h \setminus \Gamma_h} \int_F \{\boldsymbol{\nu} \Pi_2(\nabla q)\} \cdot \llbracket q \rrbracket &\lesssim \left(\sum_{F \in \mathcal{F}_h \setminus \Gamma_h} \|\sigma_F^{-1/2} \boldsymbol{\nu} (\Pi_2(\nabla q^+) + \Pi_2(\nabla q^-))\|_{L^2(F)}^2 \right)^{1/2} \\
&\quad \times \left(\sum_{F \in \mathcal{F}_h \setminus \Gamma_h} \|\sigma_F^{1/2} \llbracket q \rrbracket\|_{L^2(F)}^2 \right)^{1/2} \\
&\lesssim \varepsilon \sum_{F \in \mathcal{F}_h \setminus \Gamma_h} \left(\bar{\nu}_{E^+} \sigma_F \|\Pi_2(\nabla q^+)\|_{L^2(F)}^2 \right. \\
&\quad \left. + \bar{\nu}_{E^-} \sigma_F \|\Pi_2(\nabla q^-)\|_{L^2(F)}^2 \right) \\
&\quad + \frac{1}{4\varepsilon} \|\sigma_F^{1/2} \llbracket q \rrbracket\|_{L^2(F)}^2.
\end{aligned}$$

Employing the inverse inequality (3.2) over the simplices S_E^F and the definition of the interior penalty parameter σ , we have

$$\begin{aligned}
\sum_{F \in \mathcal{F}_h \setminus \Gamma_h} \int_F \{\boldsymbol{\nu} \Pi_2(\nabla q)\} \cdot \llbracket q \rrbracket &\lesssim \frac{\varepsilon}{\sigma_0} \sum_{E \in \mathcal{T}_h} \sum_{F \in \partial E} \frac{h_E |F|}{d|S_E^F|} \|\Pi_2(\nabla q)\|_{L^2(S_E^F)}^2 \\
&\quad + \frac{1}{4\varepsilon} \sum_{F \in \mathcal{F}_h \setminus \Gamma_h} \|\sigma_F^{1/2} \llbracket q \rrbracket\|_{L^2(F)}^2 \\
&\lesssim \frac{\varepsilon}{\sigma_0} \sum_{E \in \mathcal{T}_h} \|\boldsymbol{\nu}^{1/2} \nabla q\|_{L(E)}^2 + \frac{1}{4\varepsilon} \sum_{F \in \mathcal{F}_h \setminus \Gamma_h} \|\sigma_F^{1/2} \llbracket q \rrbracket\|_{L^2(F)}^2,
\end{aligned}$$

where we have used Assumption 3.1 and the bound (12), together with the L^2 -stability of the projector Π_2 and the property (2) of the tensor $\boldsymbol{\nu}$. In conclusion, using Assumption 3.1, we proved that

$$\tilde{\mathcal{A}}_b^{DG}(q, q) \gtrsim \|q\|_{DG}^2 \quad \text{for all } q \in V^b(h),$$

for an appropriate choice of the constant ε and for σ_0 large enough. The proof of continuity can be obtained employing analogous arguments. \square

Lemma 3.5. *The bilinear form $\mathcal{A}_\Gamma(\cdot, \cdot)$ is coercive and continuous on $V_h^\Gamma \times V_h^\Gamma$ with respect to the norm $\|\cdot\|_\Gamma$.*

Proof. Since $\mathcal{A}_\Gamma(q_h^\Gamma, q_h^\Gamma) = \|q_h^\Gamma\|_\Gamma^2$ for any $q_h^\Gamma \in V_h^\Gamma$, $\mathcal{A}_\Gamma(\cdot, \cdot)$ is clearly coercive. Continuity follows directly from Cauchy-Schwarz inequality. \square

Employing Lemma 3.4 and Lemma 3.5, we can easily prove the well-posedness of the discrete problem (11).

Proposition 3.6. *Assuming that the hypotheses of Lemmas 3.4 and 3.5 hold, problem (11) is well-posed.*

Proof. We have

$$\mathcal{I}^{DG}((q_h, q_h^\Gamma), (q, q_h^\Gamma)) = \|(q, q_h^\Gamma)\|_{\mathcal{I}}^2.$$

Moreover from Lemma 3.4 and Lemma 3.5 we know that $\tilde{\mathcal{A}}_b^{DG}(q, q) \gtrsim \|q\|_{DG}^2$ and $\mathcal{A}_\Gamma(q_h^\Gamma, q_h^\Gamma) = \|q_h^\Gamma\|_\Gamma^2$, respectively. Therefore

$$\tilde{\mathcal{A}}_h((q, q_h^\Gamma), (q, q_h^\Gamma)) \gtrsim \|(q, q_h^\Gamma)\|_{\mathcal{E}_h}^2 \quad \forall (q, q_h^\Gamma) \in V^b(h) \times V_h^\Gamma.$$

Next we prove continuity. Let $(q, q_h^\Gamma), (w, w_h^\Gamma) \in V^b(h) \times V_h^\Gamma$. Then, from Lemma 3.4 and Lemma 3.5

$$\begin{aligned} \tilde{\mathcal{A}}_b^{DG}(q, w) &\lesssim \|q\|_{DG} \|w\|_{DG} \lesssim \|(q, q_h^\Gamma)\|_{\mathcal{E}_h} \|(w, w_h^\Gamma)\|_{\mathcal{E}_h}, \\ \mathcal{A}_\Gamma(q_h^\Gamma, w_h^\Gamma) &\lesssim \|q_h^\Gamma\|_\Gamma \|w_h^\Gamma\|_\Gamma \lesssim \|(q_h, q_h^\Gamma)\|_{\mathcal{E}_h} \|(w_h, w_h^\Gamma)\|_{\mathcal{E}_h}. \end{aligned}$$

Finally, from Cauchy-Schwarz inequality, we get

$$\begin{aligned} \mathcal{I}^{DG}((q, q_h^\Gamma), (w, w_h^\Gamma)) &\leq \sum_{F \in \Gamma_h} \|\beta_\Gamma^{1/2} \llbracket q \rrbracket\|_{L^2(F)}^2 \|\beta_\Gamma^{1/2} \llbracket w \rrbracket\|_{L^2(F)}^2 \\ &\quad + \sum_{F \in \Gamma_h} \|\alpha_\Gamma^{1/2} (\{q\} - q_h^\Gamma)\|_{L^2(F)}^2 \|\alpha_\Gamma^{1/2} (\{w\} - w_h^\Gamma)\|_{L^2(F)}^2 \\ &\leq \|(q, q_h^\Gamma)\|_{\mathcal{E}_h} \|(w, w_h^\Gamma)\|_{\mathcal{E}_h}. \end{aligned}$$

The continuity of $\tilde{\mathcal{L}}_h(\cdot)$ on $V^b(h) \times V_h^\Gamma$ can be easily proved using Cauchy-Schwarz inequality, thanks to the regularity assumptions on the forcing terms f and f_Γ . □

Remark 2. The choice of employing a conforming finite element approximation for the flow in the fracture has been made in order to keep the analysis of the numerical method as clear as possible. We remark that DG methods could be employed for the fracture problem as well.

4 Error estimates

4.1 Approximation results

Approximation results in the space of polynomials are a fundamental ingredient for the error analysis of DG methods. In [24, 23, 4] standard

results on simplices are extended to polytopic elements, considering appropriate coverings and submeshes made of d -dimensional simplices (where standard results can be applied) and using appropriate extension operators. In [21] these results are extended in order to be successfully applied also in the case when the number of edges/faces is unbounded. Here we summarize the results contained in [24, 23, 4, 21].

Definition 4.1. [24, 23] A *covering* $\mathcal{T}_\# = \{T_E\}$ related to the polytopic mesh \mathcal{T}_h is a set of shape-regular d -dimensional simplices T_E , such that for each $E \in \mathcal{T}_h$, there exists a $T_E \in \mathcal{T}_\#$ such that $E \subsetneq T_E$.

Assumption 4.1. *There exists a covering $\mathcal{T}_\#$ of \mathcal{T}_h and a positive constant O_Ω , independent of the mesh parameters, such that*

$$\max_{E \in \mathcal{T}_h} O_E \leq O_\Omega,$$

where, for $E \in \mathcal{T}_h$, $O_E = \text{card}\{E' \in \mathcal{T}_h : E' \cap T_E \neq \emptyset, T_E \in \mathcal{T}_\# \text{ s.t. } E \subset T_E\}$.

For $v = (v_1, v_2) \in H^s(\Omega_1) \times H^s(\Omega_2)$, $s \geq 0$, we define the continuous extension operators $\mathcal{E}_i : H^s(\Omega_i) \rightarrow H^s(\mathbb{R}^d)$, $i = 1, 2$, cf. [38], and set $\mathcal{E}v = \mathcal{E}_1 v_1 + \mathcal{E}_2 v_2$. Clearly, $\mathcal{E}v$ is also continuous, i.e., $\|\mathcal{E}v\|_{H^s(\mathbb{R}^d)}^2 = \|\mathcal{E}_1 v_1\|_{H^s(\mathbb{R}^d)}^2 + \|\mathcal{E}_2 v_2\|_{H^s(\mathbb{R}^d)}^2 \lesssim \|v_1\|_{H^s(\Omega_1)}^2 + \|v_2\|_{H^s(\Omega_2)}^2$. We can then state the following approximation result.

Lemma 4.2. [24, 23, 4, 21] *Let $E \in \mathcal{T}_h$, $F \subset \partial E$ denote one of its faces, and $T_E \in \mathcal{T}_\#$ denote the corresponding simplex such that $E \subset T_E$ (see Definition 4.1). Suppose that $v \in L^2(\Omega)$ is such that $\mathcal{E}v|_{T_E} \in H^{r_E}(T_E)$, for some $r_E \geq 0$. Then, if Assumption 3.1 and 4.1 are satisfied, there exists $\tilde{\Pi}v$, such that $\tilde{\Pi}v|_E \in \mathbb{P}_{k_E}(E)$, and the following bound holds*

$$\|v - \tilde{\Pi}v\|_{H^q(E)} \lesssim \frac{h_E^{s_E - q}}{k_E^{r_E - q}} \|\mathcal{E}v\|_{H^{r_E}(T_E)}, \quad 0 \leq q \leq r_E. \quad (17)$$

Moreover, if $r_E > 1/2$,

$$\|v - \tilde{\Pi}v\|_{L^2(\partial E)} \lesssim \frac{h_E^{s_E - 1/2}}{k_E^{r_E - 1/2}} \|\mathcal{E}v\|_{H^{r_E}(T_E)}. \quad (18)$$

Here, $s_E = \min(k_E + 1, r_E)$ and the hidden constants depend on the shape-regularity of T_E , but are independent of v , h_E , k_E and the number of faces per element.

Proof. See [24] for a detailed proof of (17) and [21] for the proof of (18). \square

Note that the fact that estimate (18) holds on the whole boundary ∂E is fundamental for treating the case when the number of faces/edges is not uniformly bounded.

Finally, for future use, we recall that, using classical interpolation estimates [11], for any $p_\Gamma \in H^r(\Gamma_h)$, $r \geq 1$, there exists $p_\Gamma^I \in V_h^\Gamma$ such that

$$\|p_\Gamma - p_\Gamma^I\|_\Gamma \lesssim \sum_{F \in \Gamma_h} \frac{h_F^s}{k^{r-1}} |p_\Gamma|_{H^r(F)}, \quad (19)$$

with $s = \min\{k+1, r\}$.

4.2 Error analysis

In this section we will show that the discrete solution (p_h, p_h^Γ) to problem (11) (or, equivalently, to problem (14)) converges to the exact solution (p, p_Γ) , deriving an *a priori* estimate for the error in the norm (15). We point out that Galerkin's orthogonality does not hold true, due to the inconsistency of the bilinear form $\tilde{\mathcal{A}}_h$. Thereby, the error bound will be derived starting from Strang's second lemma (see [39]). From Proposition 3.6 and Strang's second lemma we directly obtain the following abstract error bound on the error.

Lemma 4.3. *Assuming that the hypotheses of Proposition 3.6 are satisfied, it holds*

$$\begin{aligned} \|(p, p_\Gamma) - (p_h, p_h^\Gamma)\|_{\mathcal{E}_h} &\lesssim \inf_{(q_h, q_h^\Gamma) \in V_h^b \times V_h^\Gamma} \|(p, p_\Gamma) - (q_h, q_h^\Gamma)\|_{\mathcal{E}_h} \\ &\quad + \sup_{(w_h, w_h^\Gamma) \in V_h^b \times V_h^\Gamma} \frac{|\mathcal{R}_h((p, p_\Gamma), (w_h, w_h^\Gamma))|}{\|(w_h, w_h^\Gamma)\|_{\mathcal{E}_h}}, \end{aligned}$$

where the residual \mathcal{R}_h is defined as

$$\mathcal{R}_h((p, p_\Gamma), (w_h, w_h^\Gamma)) = \tilde{\mathcal{A}}_h((p, p_\Gamma), (w_h, w_h^\Gamma)) - \mathcal{L}_h(w_h, w_h^\Gamma).$$

We now have all the ingredients to prove the following error estimate:

Theorem 4.4. *Let (p, p_Γ) be the solution of problem (9) and $(p_h, p_h^\Gamma) \in V_h^b \times V_h^\Gamma$ be its approximation obtained with the method (14) with the penalization parameter given by (16) and σ_0 sufficiently large. Moreover, suppose that the exact solution (p, p_Γ) is regular enough, such*

that $\mathcal{E}p|_{T_E} \in H^{r_E}(T_E)$, where \mathcal{E} is the continuous extension operator of Lemma 4.2, $r_E \geq 1 + d/2$ and $T_E \in \mathcal{T}_\#$ with $E \subset T_E$, and such that $p_\Gamma \in H^r(\Gamma_h)$, $r \geq 1$. Then, the following error bound holds:

$$\begin{aligned} \|(p, p_\Gamma) - (p_h, p_h^\Gamma)\|_{\mathcal{E}_h}^2 &\lesssim \sum_{E \in \mathcal{T}_h} \frac{h_E^{2(s_E-1)}}{k_E^{2(r_E-1)}} G_E(h_E, k_E, \bar{\nu}_E) \|\mathcal{E}p\|_{H^{r_E}(T_E)}^2 \\ &\quad + \sum_{F \in \Gamma_h} \frac{h_F^{2k}}{k^{2(r-1)}} |p_\Gamma|_{H^r(F)}^2, \end{aligned}$$

Here, $s_E = \min(k_E + 1, r_E)$ and

$$\begin{aligned} G_E(h_E, k_E, \bar{\nu}_E) &= \bar{\nu}_E + h_E k_E^{-1} \max_{F \subset \partial E \setminus \Gamma} \sigma_F + (\alpha_\Gamma + \beta_\Gamma) h_E k_E^{-1} \\ &\quad + \bar{\nu}_E h_E^{-1} k_E \max_{F \subset \partial E \setminus \Gamma} \sigma_F^{-1} + \bar{\nu}_E h_E^{-1} k_E^2 \max_{F \subset \partial E \setminus \Gamma} \sigma_F^{-1}. \end{aligned}$$

Proof. From Lemma 4.3 we know that the error satisfies the following bound

$$\begin{aligned} \|(p, p_\Gamma) - (p_h, p_h^\Gamma)\|_{\mathcal{E}_h} &\lesssim \underbrace{\inf_{(q_h, q_h^\Gamma) \in V_h^b \times V_h^\Gamma} \|(p, p_\Gamma) - (q_h, q_h^\Gamma)\|_{\mathcal{E}_h}}_I \\ &\quad + \underbrace{\sup_{(w_h, w_h^\Gamma) \in V_h^b \times V_h^\Gamma} \frac{|\mathcal{R}_h((p, p_\Gamma), (w_h, w_h^\Gamma))|}{\|(w_h, w_h^\Gamma)\|_{\mathcal{E}_h}}}_{II}. \quad (20) \end{aligned}$$

We bound the two terms on the right-hand side of (20) separately. We can rewrite term I as

$$\begin{aligned} I &= \underbrace{\inf_{q_h \in V_h^b} \|p - q_h\|_{DG}^2}_{(a)} + \underbrace{\inf_{q_h^\Gamma \in V_h^\Gamma} \|p_\Gamma - q_h^\Gamma\|_{\Gamma}^2}_{(b)} \\ &\quad + \underbrace{\inf_{(q_h, q_h^\Gamma) \in V_h^b \times V_h^\Gamma} \|(p - q_h, p_\Gamma - q_h^\Gamma)\|_{\mathcal{I}}^2}_{(c)}. \end{aligned}$$

Again we consider each of the three terms separately. To bound term (a), we

exploit the two approximation results stated in Lemma 4.2; we obtain that

$$\begin{aligned}
(a) &\leq \|p - \tilde{\Pi}p\|_{DG}^2 = \sum_{E \in \mathcal{T}_h} \|\nu^{1/2} \nabla(p - \tilde{\Pi}p)\|_{L^2(E)}^2 + \sum_{F \in \mathcal{F}_h \setminus \Gamma_h} \sigma_F \| [p - \tilde{\Pi}p] \|_{L^2(F)}^2 \\
&\lesssim \sum_{E \in \mathcal{T}_h} \left[\bar{\nu}_E |p - \tilde{\Pi}p|_{H^1(E)}^2 + \left(\max_{F \subset \partial E \setminus \Gamma} \sigma_F \right) \|p - \tilde{\Pi}p\|_{L^2(\partial E \setminus \Gamma)}^2 \right] \\
&\lesssim \sum_{E \in \mathcal{T}_h} \left[\frac{h_E^{2(s_E-1)}}{k_E^{2(r_E-1)}} \bar{\nu}_E \|\mathcal{E}p\|_{H^{r_E}(T_E)}^2 \right. \\
&\quad \left. + \sum_{F \subset \partial E \setminus \Gamma} \frac{h_E^{2(s_E-1/2)}}{k_E^{2(r_E-1/2)}} \left(\max_{F \subset \partial E \setminus \Gamma} \sigma_F \right) \|\mathcal{E}p\|_{H^{r_E}(T_E)}^2 \right] \\
&= \sum_{E \in \mathcal{T}_h} \frac{h_E^{2(s_E-1)}}{k_E^{2(r_E-1)}} \|\mathcal{E}p\|_{H^{r_E}(T_E)}^2 \left(\bar{\nu}_E + \frac{h_E}{k_E} \left(\max_{F \subset \partial E \setminus \Gamma} \sigma_F \right) \right).
\end{aligned}$$

Using classical interpolation estimates (see (19)) we can bound term (b) as follows:

$$(b) \leq \|p_\Gamma - p_\Gamma^I\|_\Gamma^2 \lesssim \sum_{F \in \Gamma_h} \frac{h_F^{2k}}{k^{2(r-1)}} |p_\Gamma|_{H^r(F)}^2.$$

Finally, for term (c), we have

$$\begin{aligned}
(c) \leq \| (p - \tilde{\Pi}p, p_\Gamma - p_\Gamma^I) \|_{\mathcal{I}}^2 &\leq \beta_\Gamma \sum_{F \in \Gamma_h} \| [p - \tilde{\Pi}p] \|_{L^2(F)}^2 + \alpha_\Gamma \sum_{F \in \Gamma_h} \| \{p - \tilde{\Pi}p\} \|_{L^2(F)}^2 \\
&\quad + \alpha_\Gamma \sum_{F \in \Gamma_h} \| p_\Gamma - p_\Gamma^I \|_{L^2(F)}^2.
\end{aligned}$$

Exploiting the approximation result (18), we obtain

$$\begin{aligned}
\beta_\Gamma \sum_{F \in \Gamma_h} \| [p - \tilde{\Pi}p] \|_{L^2(F)}^2 &\leq \beta_\Gamma \sum_{\substack{E \in \mathcal{T}_h \\ \partial E \cap \Gamma \neq \emptyset}} \| p - \tilde{\Pi}p \|_{L^2(\partial E)}^2 \\
&\lesssim \beta_\Gamma \sum_{\substack{E \in \mathcal{T}_h \\ \partial E \cap \Gamma \neq \emptyset}} \frac{h_E^{2(s_E-1/2)}}{k_E^{2(r_E-1/2)}} \|\mathcal{E}p\|_{H^{r_E}(T_E)}^2 \\
&= \beta_\Gamma \sum_{\substack{E \in \mathcal{T}_h \\ \partial E \cap \Gamma \neq \emptyset}} \frac{h_E^{2(s_E-1)}}{k_E^{2(r_E-1)}} \|\mathcal{E}p\|_{H^{r_E}(T_E)}^2 \frac{h_E}{k_E}.
\end{aligned}$$

Similarly, we have

$$\alpha_\Gamma \sum_{F \in \Gamma_h} \|\{p - \tilde{\Pi}p\}\|_{L^2(F)}^2 \lesssim \alpha_\Gamma \sum_{\substack{E \in \mathcal{T}_h \\ \partial E \cap \Gamma \neq \emptyset}} \frac{h_E^{2(s_E-1)}}{k_E^{2(r_E-1)}} \frac{h_E}{k_E} \|\mathcal{E}p\|_{H^r(T_E)}^2.$$

Finally, using again classical interpolation estimates, we deduce that

$$\alpha_\Gamma \sum_{F \in \Gamma_h} \|p_\Gamma - p_\Gamma^I\|_{L^2(F)}^2 \lesssim \sum_{e \in \Gamma_h} \frac{h_F^{2k}}{k^{2(r-1)}} |p_\Gamma|_{H^r(F)}^2.$$

In conclusion, combining all the previous estimates, we can bound the term I on the right-hand side of (20) as follows:

$$\begin{aligned} I \lesssim & \sum_{F \in \Gamma_h} h_F^{2k} |p_\Gamma|_{H^{k+1}(F)}^2 \\ & + \sum_{E \in \mathcal{T}_h} \frac{h_E^{2(s_E-1)}}{k_E^{2(r_E-1)}} \|\mathcal{E}p\|_{H^r(T_E)}^2 \left[\bar{\nu}_E + h_E k_E^{-1} \left(\max_{F \subset \partial E \setminus \Gamma} \sigma_F \right) \right. \\ & \left. + (\alpha_\Gamma + \beta_\Gamma) h_E k_E^{-1} \right]. \quad (21) \end{aligned}$$

Next, we derive a bound on the term II on the right-hand side of (20). First, we note that, integrating by parts elementwise and using that the couple (p, p_Γ) satisfies (9), we can rewrite the residual \mathcal{R}_h as

$$\mathcal{R}_h((p, p_\Gamma), (w_h, w_h^\Gamma)) = \sum_{F \in \mathcal{F}_h \setminus \Gamma_h} \int_F \{\boldsymbol{\nu}(\nabla p - \Pi_2(\nabla p))\} \cdot \llbracket w_h \rrbracket.$$

Employing Cauchy-Schwarz inequality and the definition of the norm $\|\cdot\|_{\mathcal{E}_h}$, we then obtain

$$II \leq \left(\sum_{F \in \mathcal{F}_h \setminus \Gamma_h} \sigma_F^{-1} \int_F |\{\boldsymbol{\nu}(\nabla p - \Pi_2(\nabla p))\}|^2 \right)^{1/2}.$$

If we still denote by $\tilde{\Pi}$ the vector-valued generalization of the projection operator $\tilde{\Pi}$ defined in Lemma 4.2, we observe that

$$\begin{aligned} \sum_{F \in \mathcal{F}_h \setminus \Gamma_h} \sigma_F^{-1} \int_F |\{\boldsymbol{\nu}(\nabla p - \Pi_2(\nabla p))\}|^2 & \leq \sum_{F \in \mathcal{F}_h \setminus \Gamma_h} \sigma_F^{-1} \int_F |\{\boldsymbol{\nu}(\nabla p - \tilde{\Pi}(\nabla p))\}|^2 \\ & + \sum_{F \in \mathcal{F}_h \setminus \Gamma_h} \sigma_F^{-1} \int_F |\{\boldsymbol{\nu} \Pi_2(\nabla p - \tilde{\Pi}(\nabla p))\}|^2 \\ & \equiv (1) + (2). \end{aligned}$$

To bound term (1), we proceed as above, employing the approximation result stated in Lemma 4.2. We obtain

$$(1) \lesssim \sum_{E \in \mathcal{T}_h} \frac{h_E^{2(s_E-1)}}{k_E^{2(r_E-1)}} (\bar{\nu}_E (\max_{F \subset \partial E \setminus \Gamma} \sigma_F^{-1}) \frac{h_E^{-1}}{k_E^{-1}}) \|\mathcal{E}p\|_{H^{r_E}(T_E)}^2.$$

Exploiting, in order, the boundedness of the permeability tensor (2), the inverse inequality (13), the L^2 -stability of the projector Π_2 and the approximation results stated in Lemma 4.2, we can bound term (2) as follows:

$$\begin{aligned} (2) &\lesssim \sum_{E \in \mathcal{T}_h} (\max_{F \subset \partial E \setminus \Gamma} \sigma_F^{-1}) \bar{\nu}_E \|\Pi_2(\tilde{\Pi}(\nabla p) - \nabla p)\|_{L^2(\partial E \setminus \Gamma)}^2 \\ &\lesssim \sum_{E \in \mathcal{T}_h} (\max_{F \subset \partial E \setminus \Gamma} \sigma_F^{-1}) \bar{\nu}_E \frac{k_E^2}{h_E} \|\tilde{\Pi}(\nabla p) - \nabla p\|_{L^2(E)}^2 \\ &\lesssim \sum_{E \in \mathcal{T}_h} \frac{h_E^{2(s_E-1)}}{k_E^{2(r_E-1)}} \|\mathcal{E}p\|_{H^{r_E}(T_E)}^2 \left(\bar{\nu}_E \frac{k_E^2}{h_E} (\max_{F \subset \partial E \setminus \Gamma} \sigma_F^{-1}) \right). \end{aligned}$$

Hence, the term II on the right-hand side of (20) may be bounded as:

$$\begin{aligned} II \lesssim \sum_{E \in \mathcal{T}_h} \frac{h_E^{2(s_E-1)}}{k_E^{2(r_E-1)}} \|\mathcal{E}p\|_{H^{r_E}(T_E)}^2 &\left[\bar{\nu}_E (\max_{F \subset \partial E \setminus \Gamma} \sigma_F^{-1}) h_E^{-1} k_E \right. \\ &\left. + \bar{\nu}_E (\max_{F \subset \partial E \setminus \Gamma} \sigma_F^{-1}) h_E^{-1} k_E^2 \right]. \quad (22) \end{aligned}$$

Finally, substituting (21) and (22) into (20), leads to the thesis. \square

5 Numerical results

In this section we present some two-dimensional numerical experiments to confirm the validity of the *a priori* error estimates that we have derived for our method. The numerical results have been obtained in MATLAB[®]. Throughout this section we set the fracture thickness (appearing in the coupling conditions (6a)-(6b)) equal to $\ell_\Gamma = 0.001 = \eta_\Gamma$ and $\nu_\Gamma^\tau = 1$. For the generation of polygonal meshes conforming to the fractures we have suitably modified the MATLAB[®] code `PolyMesher` developed by G.H. Paulino and collaborators [40].

5.1 Example 1

In this first test case we take $\Omega = (0, 1)^2$, and choose as exact solutions in the bulk and in the fracture $\Gamma = \{(x, y) \in \Omega : x + y = 1\}$ as

$$p = \begin{cases} e^{x+y} & \text{in } \Omega_1, \\ e^{x+y} + \frac{4\eta_\Gamma}{\sqrt{2}}e & \text{in } \Omega_2, \end{cases} \quad p_\Gamma = e + \frac{2\eta_\Gamma}{\sqrt{2}}e.$$

It is easy to prove that p and p_Γ satisfy the coupling conditions (6a)-(6b) with $\xi = 1$ and $\boldsymbol{\nu} = \mathbf{I}$. Note that in this case $f_\Gamma = 0$ since the solution is constant and $[\boldsymbol{\nu}\nabla p] = 0$.

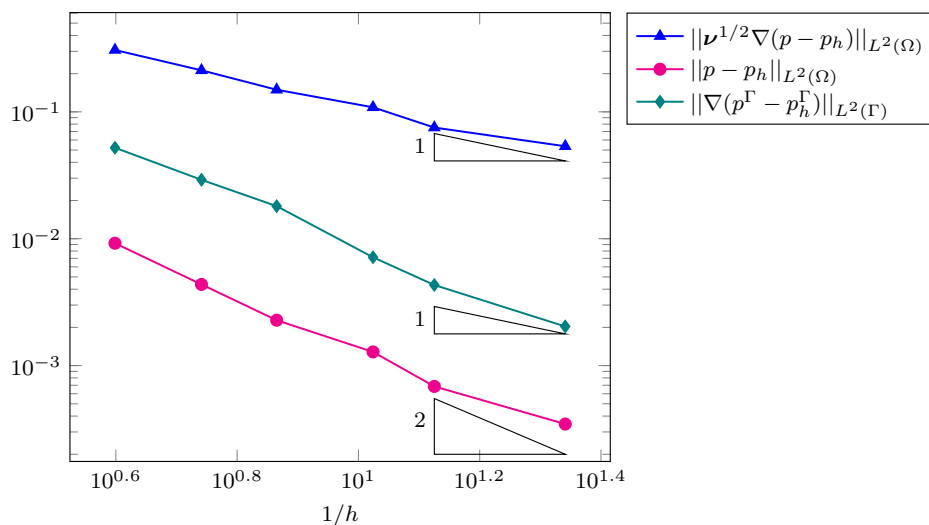


Figure 3: Example 1: Computed errors in the bulk and in the fracture as a function of the inverse of the mesh size (loglog scale) with polynomial degree $k = 1$.

In Figure 3 we plot the computed errors $\|\boldsymbol{\nu}^{1/2}\nabla(p - p_h)\|_{L^2(\Omega)}$ and $\|\nabla(p^\Gamma - p_h^\Gamma)\|_{L^2(\Gamma)}$ as a function of inverse of the mesh size (loglog scale). The sequence of computational grids are shown in Figure 5. Here we have taken the polynomial degree $k_E = 1 \forall E \in \mathcal{T}_h$ and $k = 1$ for the fracture finite dimensional space. In both cases the numerical results are in agreement with the theoretical estimates, i.e., the error goes to zero at a rate $\mathcal{O}(h)$. In the same plot we also report the behaviour of the error $\|p - p_h\|_{L^2(\Omega)}$. One order of convergence is clearly gained. Finally, in Figure 4 we report the computed errors in the bulk $\|\boldsymbol{\nu}^{1/2}\nabla(p - p_h)\|_{L^2(\Omega)}$ as a function of h for $k_E = k = 1, 2, 3$. The theoretical convergence rates are clearly achieved.

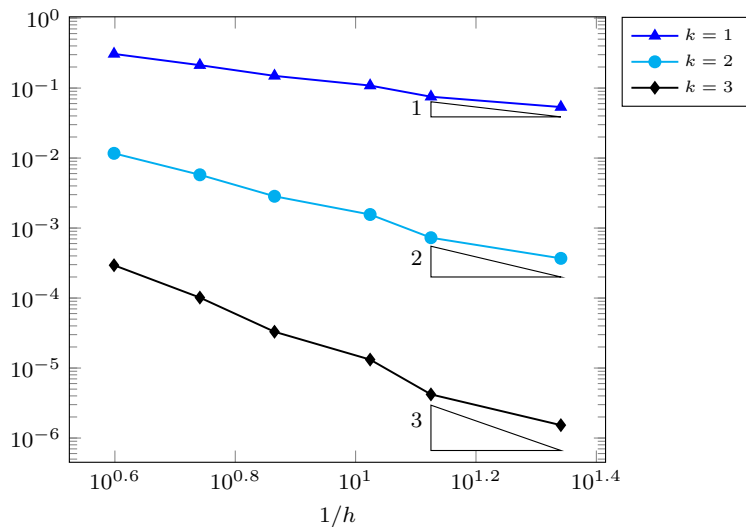


Figure 4: Example 1: Computed errors $\|\nu^{1/2}\nabla(p - p_h)\|_{L^2(\Omega)}$ in the bulk as a function of the inverse of the mesh size (loglog scale) for polynomial degrees $k = 1, 2, 3$.

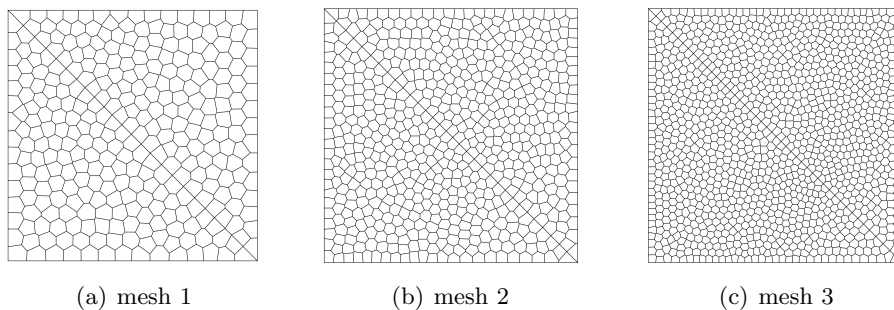


Figure 5: Example 1: Three refinements of the polygonal mesh grid conforming to the fracture.

5.2 Example 2

Here we consider again $\Omega = (0, 1)^2$ and $\Gamma = \{(x, y) \in \Omega : x + y = 1\}$. We take as exact solutions in the bulk and in the fracture

$$p = \begin{cases} e^{x+y} & \text{in } \Omega_1, \\ \frac{e^{x+y}}{2} + \left(\frac{1}{2} + \frac{3\eta_\Gamma}{\sqrt{2}}\right)e & \text{in } \Omega_2, \end{cases} \quad p_\Gamma = e(1 + \sqrt{2}\eta_\Gamma).$$

We choose $\xi = 1$ and take again $\boldsymbol{\nu} = \mathbf{I}$. In this case we set the source term as

$$f = \begin{cases} -2e^{x+y} & \text{in } \Omega_1, \\ \frac{c}{\sqrt{2}} & \text{in } \Gamma, \\ -e^{x+y} & \text{in } \Omega_2. \end{cases}$$

Notice that on the fracture the source term satisfies $f_\Gamma = -\nabla_\tau \cdot (\boldsymbol{\nu}_\Gamma^\tau \ell_\Gamma \nabla_\tau p_\Gamma) + \llbracket \boldsymbol{\nu} \nabla p \rrbracket$, and, since p_Γ is constant, it holds $f_\Gamma = \llbracket \boldsymbol{\nu} \nabla p \rrbracket$.

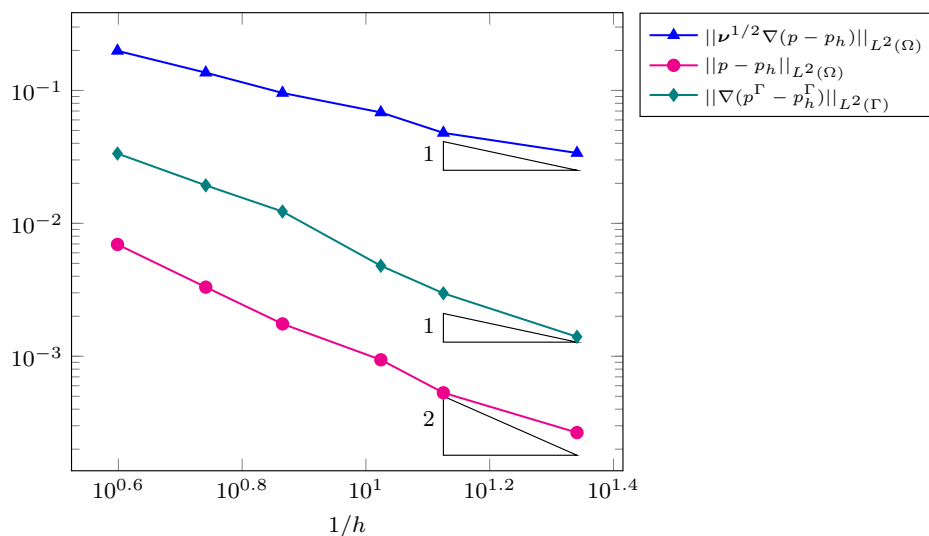


Figure 6: Example 2: Computed errors in the bulk and in the fracture as a function of the inverse of the mesh size (loglog scale) with polynomial degree $k = 1$.

Figure 6 shows the computed errors $\|\boldsymbol{\nu}^{1/2} \nabla(p - p_h)\|_{L^2(\Omega)}$ for the bulk problem and the corresponding computed errors $\|\nabla(p^\Gamma - p_h^\Gamma)\|_{L^2(\Gamma)}$ in the fracture. The results have been obtained taking the polynomial degree $k = 1$ for both the bulk and fracture problems. As predicted from our theoretical error bounds, a convergence of order 1 is clearly observed for both $\|\boldsymbol{\nu}^{1/2} \nabla(p - p_h)\|_{L^2(\Omega)}$ and $\|\nabla(p^\Gamma - p_h^\Gamma)\|_{L^2(\Gamma)}$. Moreover from Figure 6 one can clearly see that also in this test case one order of convergence is gained if we compute the error $\|p - p_h\|_{L^2(\Omega)}$. In Figure 7 we plot the computed errors in the bulk $\|\boldsymbol{\nu}^{1/2} \nabla(p - p_h)\|_{L^2(\Omega)}$ for polynomial degrees $k_E = k = 1, 2, 3$. They are in agreement with the expected convergence rates of $\mathcal{O}(h^k)$.

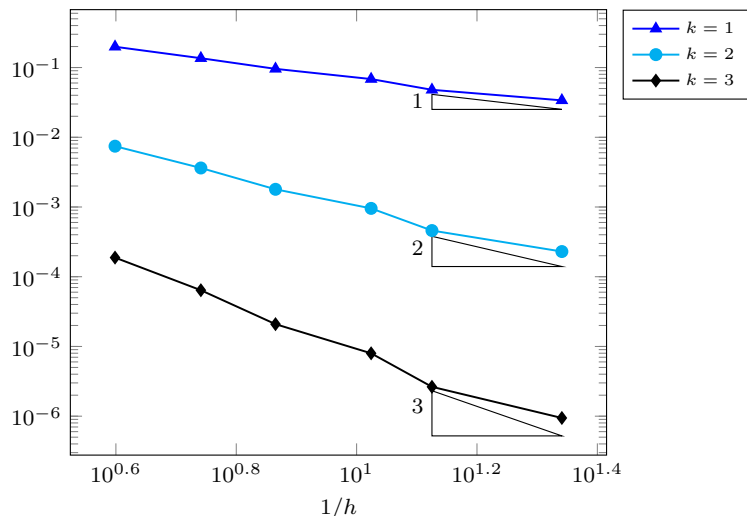


Figure 7: Example 2: Computed errors $\|\nu^{1/2}\nabla(p - p_h)\|_{L^2(\Omega)}$ in the bulk as a function of the inverse of the mesh size (loglog scale) for polynomial degrees $k = 1, 2, 3$.

5.3 Example 3

In this last example we consider the circular fracture $\Gamma = \{(x, y) \in \Omega : x^2 + y^2 = R\}$, with $R = 0.7$ included in the domain $\Omega = (0, 1)^2$. We choose the exact solutions in the bulk and in the fracture as follows

$$p = \begin{cases} \frac{x^2 + y^2}{R^2} & \text{in } \Omega_1, \\ \frac{x^2 + y^2}{2R^2} + \frac{3}{R}\eta_\Gamma + \frac{1}{2} & \text{in } \Omega_2, \end{cases} \quad p_\Gamma = 1 + \frac{7}{4}\frac{\eta_\Gamma}{R},$$

so that they satisfy the coupling conditions (6a)-(6b) with $\xi = \frac{3}{4}$ and $\nu = \mathbf{I}$. The source term is chosen as

$$f = \begin{cases} -\frac{4}{R^2} & \text{in } \Omega_1, \\ \frac{1}{R} & \text{in } \Gamma, \\ -\frac{2}{R^2} & \text{in } \Omega_2. \end{cases}$$

Figure 8 shows three successive levels of refinements employed in this set of experiments. One can see that here the fracture is approximated by a polygonal line.

In Figure 9 we report the computed errors $\|\nu^{1/2}\nabla(p - p_h)\|_{L^2(\Omega)}$ and $\|\nabla(p^\Gamma - p_h^\Gamma)\|_{L^2(\Gamma)}$ as a function of $1/h$ for $k_E = k = 1$ (we disregard

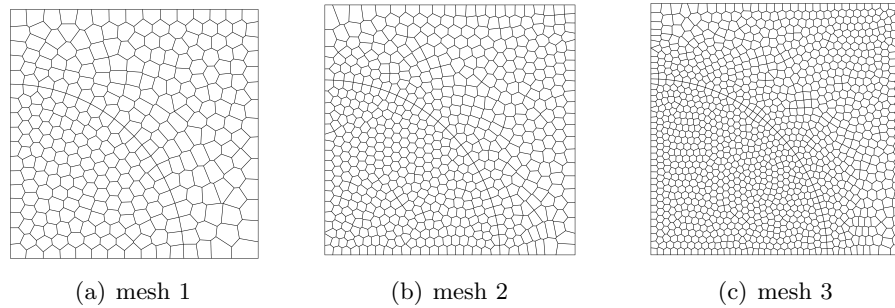


Figure 8: Example 3: Three refinements of the polygonal mesh grid with circular fracture.

the variational crime coming from the polygonal approximation of the circular fracture). The numerical experiments validate the theoretical estimates, as a linear decay of the error is clearly observed.

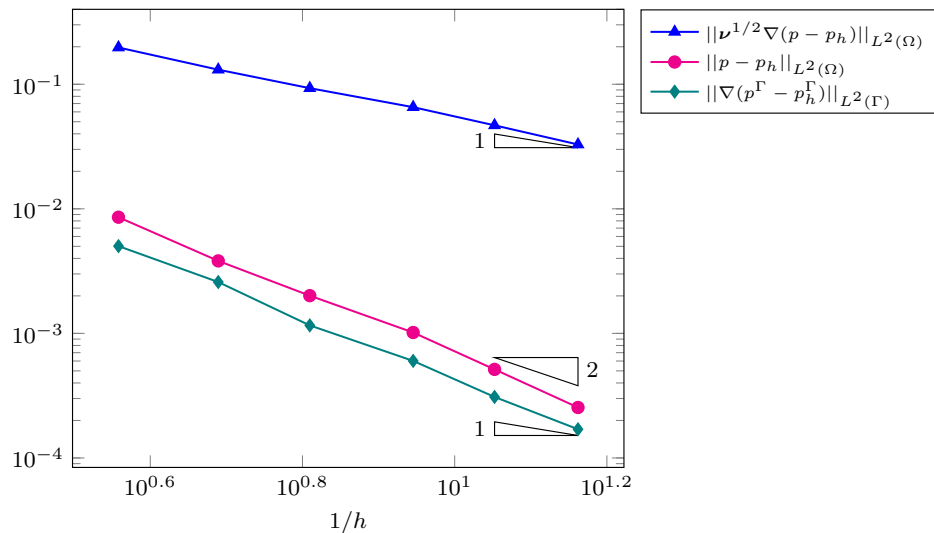


Figure 9: Example 3: Computed errors as a function of inverse of the mesh size (loglog scale) with polynomial degree $k = 1$.

References

- [1] C. Alboin, J. Jaffré, J. E. Roberts, and C. Serres. Modeling fractures as interfaces for flow and transport in porous media. In *Fluid flow*

- and transport in porous media: mathematical and numerical treatment (South Hadley, MA, 2001)*, volume 295 of *Contemp. Math.*, pages 13–24. Amer. Math. Soc., Providence, RI, 2002.
- [2] C. Alboin, J. Jaffré, J. E. Roberts, X. Wang, and C. Serres. Domain decomposition for some transmission problems in flow in porous media. In *Numerical treatment of multiphase flows in porous media*, volume 552 of *Lecture Notes in Phys.*, pages 22–34. Springer, Berlin, 2000.
 - [3] P. Angot, F. Boyer, and F. Hubert. Asymptotic and numerical modelling of flows in fractured porous media. *M2AN Math. Model. Numer. Anal.*, 43(2):239–275, 2009.
 - [4] P. F. Antonietti, A. Cangiani, J. Collis, Z. Dong, E. H. Georgoulis, S. Giani, and P. Houston. *Review of discontinuous Galerkin finite element methods for partial differential equations on complicated domains*. Lecture Notes in Computational Science and Engineering, 2016.
 - [5] P. F. Antonietti, L. Formaggia, A. Scotti, M. Verani, and N. Verzotti. Mimetic finite difference approximation of flows in fractured porous media. *M2AN Math. Model. Numer. Anal.*, 50(3):809–832, 2016.
 - [6] P. F. Antonietti, S. Giani, and P. Houston. *hp*-version composite discontinuous Galerkin methods for elliptic problems on complicated domains. *SIAM Journal on Scientific Computing*, 35(3):A1417–A1439, 2013.
 - [7] P. F. Antonietti, S. Giani, and P. Houston. Domain decomposition preconditioners for discontinuous Galerkin methods for elliptic problems on complicated domains. *Journal of Scientific Computing*, 60(1):203–227, 2014.
 - [8] P. F. Antonietti, P. Houston, X. Hu, M. Sarti, and M. Verani. Multi-grid algorithms for *hp*-version interior penalty discontinuous Galerkin methods on polygonal and polyhedral meshes. *arXiv preprint:1412.0913*, 2014.
 - [9] D. N. Arnold. An interior penalty finite element method with discontinuous elements. *SIAM J. Numer. Anal.*, 19(4):742–760, 1982.
 - [10] D. N. Arnold, F. Brezzi, B. Cockburn, and L. D. Marini. Unified analysis of discontinuous Galerkin methods for elliptic problems. *SIAM J. Numer. Anal.*, 39(5):1749–1779, 2001/02.

- [11] I. Babuška and M. Suri. The hp version of the finite element method with quasi-uniform meshes. *RAIRO-Modélisation mathématique et analyse numérique*, 21(2):199–238, 1987.
- [12] G. A. Baker. Finite element methods for elliptic equations using non-conforming elements. *Math. Comp.*, 31(137):45–59, 1977.
- [13] F. Bassi and S. Rebay. A high-order accurate discontinuous finite element method for the numerical solution of the compressible Navier-Stokes equations. *J. Comput. Phys.*, 131(2):267–279, 1997.
- [14] J. Bear, C. F. Tsang, and G. d. Marsily. Flow and contaminant transport in fractured rocks. *Academic Press, San Diego*, 1993.
- [15] M. F. Benedetto, S. Berrone, and S. Scialò. A globally conforming method for solving flow in discrete fracture networks using the virtual element method. *Finite Elements in Analysis and Design*, 109:23–36, 2016.
- [16] S. Berrone, S. Pieraccini, and S. Scialò. On simulations of discrete fracture network flows with an optimization-based extended finite element method. *SIAM Journal on Scientific Computing*, 35(2):A908–A935, 2013.
- [17] S. Berrone, S. Pieraccini, and S. Scialò. A PDE-constrained optimization formulation for discrete fracture network flows. *SIAM J. Sci. Comput.*, 35(2):B487–B510, 2013.
- [18] S. Berrone, S. Pieraccini, and S. Scialò. An optimization approach for large scale simulations of discrete fracture network flows. *J. Comput. Phys.*, 256:838–853, 2014.
- [19] S. Berrone, S. Pieraccini, S. Scialò, and F. Vicini. A parallel solver for large scale DFN flow simulations. *SIAM J. Sci. Comput.*, 37(3):C285–C306, 2015.
- [20] F. Brezzi, B. Cockburn, L. D. Marini, and E. Süli. Stabilization mechanisms in discontinuous Galerkin finite element methods. *Comput. Methods Appl. Mech. Engrg.*, 195(25-28):3293–3310, 2006.
- [21] A. Cangiani, Z. Dong, and E. H. Georgoulis. hp -version space-time discontinuous Galerkin methods for parabolic problems on prismatic meshes. *arXiv preprint:1605.01212*, 2016.

- [22] A. Cangiani, Z. Dong, E. H. Georgoulis, and P. Houston. *hp-version discontinuous Galerkin methods on polytopic meshes*. to appear.
- [23] A. Cangiani, Z. Dong, E. H. Georgoulis, and P. Houston. *hp-version discontinuous Galerkin methods for advection-diffusion-reaction problems on polytopic meshes*. *ESAIM Math. Model. Numer. Anal.*, 50(3):699–725, 2016.
- [24] A. Cangiani, E. H. Georgoulis, and P. Houston. *hp-version discontinuous Galerkin methods on polygonal and polyhedral meshes*. *Math. Models Methods Appl. Sci.*, 24(10):2009–2041, 2014.
- [25] P. Castillo, B. Cockburn, I. Perugia, and D. Schötzau. An a priori error analysis of the local discontinuous Galerkin method for elliptic problems. *SIAM J. Numer. Anal.*, 38(5):1676–1706, 2000.
- [26] B. Cockburn and C. Dawson. Some extensions of the local discontinuous Galerkin method for convection-diffusion equations in multidimensions. In *The mathematics of finite elements and applications, X, MAFELAP 1999 (Uxbridge)*, pages 225–238. Elsevier, Oxford, 2000.
- [27] C. D’Angelo and A. Scotti. A mixed finite element method for darcy flow in fractured porous media with non-matching grids. *ESAIM: Mathematical Modelling and Numerical Analysis*, 46(02):465–489, 2012.
- [28] D. A. Di Pietro and A. Ern. *Mathematical aspects of discontinuous Galerkin methods*, volume 69. Springer Science & Business Media, 2011.
- [29] J. Douglas, Jr. and T. Dupont. Interior penalty procedures for elliptic and parabolic Galerkin methods. In *Computing methods in applied sciences (Second Internat. Sympos., Versailles, 1975)*, pages 207–216. Lecture Notes in Phys., Vol. 58. Springer, Berlin, 1976.
- [30] L. Formaggia, A. Scotti, and F. Sottocasa. Analysis of a Mimetic Finite Difference approximation of flows in fractured porous media. *Submitted*, 2016.
- [31] N. Frih, J. E. Roberts, and A. Saada. Modeling fractures as interfaces: a model for Forchheimer fractures. *Comput. Geosci.*, 12(1):91–104, 2008.
- [32] A. Fumagalli and A. Scotti. A numerical method for two-phase flow in fractured porous media with non-matching grids. *Advances in Water Resources*, 62, Part C:454–464, 2013.

- [33] J. S. Hesthaven and T. Warburton. *Nodal discontinuous Galerkin methods: algorithms, analysis, and applications*. Springer Science & Business Media, 2007.
- [34] J. Jaffré, M. Mnejja, and J. Roberts. A discrete fracture model for two-phase flow with matrix-fracture interaction. *Procedia Computer Science*, 4:967–973, 2011.
- [35] V. Martin, J. Jaffré, and J. E. Roberts. Modeling fractures and barriers as interfaces for flow in porous media. *SIAM J. Sci. Comput.*, 26(5):1667–1691, 2005.
- [36] W. Reed and T. Hill. Triangular mesh methods for the neutron transport equation. *Los Alamos Report LA-UR-73-479*, 1973.
- [37] B. Rivière. *Discontinuous Galerkin methods for solving elliptic and parabolic equations*, volume 35 of *Frontiers in Applied Mathematics*. Society for Industrial and Applied Mathematics (SIAM), Philadelphia, PA, 2008. Theory and implementation.
- [38] E. M. Stein. *Singular integrals and differentiability properties of functions*, volume 2. Princeton university press, 1970.
- [39] G. Strang and G. J. Fix. *An analysis of the finite element method*, volume 212. Prentice-Hall Englewood Cliffs, NJ, 1973.
- [40] C. Talischi, G. H. Paulino, A. Pereira, and I. F. Menezes. Polymesh: a general-purpose mesh generator for polygonal elements written in matlab. *Structural and Multidisciplinary Optimization*, 45(3):309–328, 2012.
- [41] T. Warburton and J. S. Hesthaven. On the constants in hp -finite element trace inverse inequalities. *Computer methods in applied mechanics and engineering*, 192(25):2765–2773, 2003.
- [42] M. F. Wheeler. An elliptic collocation-finite element method with interior penalties. *SIAM J. Numer. Anal.*, 15(1):152–161, 1978.

MOX Technical Reports, last issues

Dipartimento di Matematica
Politecnico di Milano, Via Bonardi 9 - 20133 Milano (Italy)

- 54/2016** Vergara, C.; Le Van, D.; Quadrio, M.; Formaggia, L.; Domanin, M.
Large Eddy Simulations of blood dynamics in abdominal aortic aneurysms
- 52/2016** Paolucci, R.; Evangelista, L.; Mazzieri, I.; Schiappapietra, E.
The 3D Numerical Simulation of Near-Source Ground Motion during the Marsica Earthquake, Central Italy, 100 years later
- 53/2016** Antonietti, P. F.; Manzini, G.; Verani, M.
The fully nonconforming Virtual Element method for biharmonic problems
- 51/2016** Guzzetti, S.; Perotto, S.; Veneziani, A.
Hierarchical Model Reduction for Incompressible Flows in Cylindrical Domains: The Axisymmetric Case
- 50/2016** Ambrosi, D.; Pezzuto, S.; Riccobelli, D.; Stylianopoulos, T.; Ciarletta, P.
Solid tumors are poroelastic solids with a chemo--mechanical feedback on growth
- 49/2016** Formaggia, L.; Scotti, A.; Sottocasa, F.
ANALYSIS OF A MIMETIC FINITE DIFFERENCE APPROXIMATION OF FLOWS IN FRACTURED POROUS MEDIA
- 48/2016** Scardulla, S.; Pasta, S.; D'Acquisto, L.; Sciacca, S.; Agnese, V.; Vergara, C.; Quarteroni, A.; C
Shear Stress Alterations in the Celiac Trunk of Patients with Continuous-Flow Left Ventricular Assist Device by In-Silico and In-Vitro Flow Analysis
- 46/2016** Lila, E.; Aston, J.A.D.; Sangalli, L.M.
Smooth Principal Component Analysis over two-dimensional manifolds with an application to Neuroimaging
- 47/2016** Canuto, C.; Nochetto, R. H.; Stevenson R.; Verani, M.
On p -Robust Saturation for hp -AFEM
- 42/2016** Iannetti, L.; D'Urso, G.; Conoscenti, G.; Cutri, E.; Tuan, R.S.; Raimondi, M.T.; Gottardi, R.; Z
Distributed and lumped parameter models for the characterization of high throughput bioreactors